metals

MDPI

Article

Comparison of the Effect of Mechanical and Ultrasonic Agitation on the Properties of Electrodeposited Ni-Co/ZrO_2 Composite Coatings

Binzhou Li [1,2], Jianming Su [3], Jidong Li [4] and Yiyong Wang [4,*]

[1] State Key Laboratory of Metal Material for Marine Equipment and Application, Anshan 114009, China
[2] Ansteel Beijing Research Institute, Beijing 102209, China
[3] Steelmaking Plant of Anshan Iron and Steel Group Co., Anshan 114000, China
[4] College of Material and Metallurgy, University of Science and Technology Liaoning, Anshan 114051, China
* Correspondence: wangyiyongfly@163.com

Abstract: Ni-Co/ZrO_2 composite coatings were fabricated by electrochemical deposition from sulfamate solutions containing zirconia nanoparticles. The main purpose of this research was to evaluate the effect of mechanical stirring and ultrasonic agitation in plating solutions on the structure and properties of Ni-Co/ZrO_2 composite coatings. The morphology, microstructure, microhardness, anti-corrosion and wear resistance of the composites were investigated via scanning electron microscopy, X-ray diffraction, Vickers microhardness testing, electrochemical workstation utilization and friction wear testing. The hardness, friction coefficient, wear loss, corrosion rate of the composite coating prepared with mechanical stirring, and ultrasonic agitation were 533 and 680 HV; 0.40 ± 0.02 and 0.35 ± 0.02; 2.15×10^{-5}; 0.85×10^{-5} g·m^{-1}; and 0.36 and 0.07 mm/year, respectively. In comparison to mechanical stirring, ultrasonic agitation could more uniformly disperse the zirconia nanoparticles to obtain Ni-Co/ZrO_2 composite coatings, which has simplicity and compactness.

Keywords: ultrasound; Ni-Co composite coating; zirconia (ZrO_2); electrodeposition; mechanical properties

check for updates

Citation: Li, B.; Su, J.; Li, J.; Wang, Y. Comparison of the Effect of Mechanical and Ultrasonic Agitation on the Properties of Electrodeposited Ni-Co/ZrO_2 Composite Coatings. *Metals* **2023**, *13*, 478. https://doi.org/10.3390/met13030478

Academic Editors: Nebojša Nikolić and Juan Creus

Received: 14 December 2022
Revised: 17 February 2023
Accepted: 20 February 2023
Published: 25 February 2023

Copyright: © 2023 by the authors. Licensee MDPI, Basel, Switzerland. This article is an open access article distributed under the terms and conditions of the Creative Commons Attribution (CC BY) license (https://creativecommons.org/licenses/by/4.0/).

1. Introduction

Recently, numerous studies have been conducted on composite coatings that contain inert particles as a result of their excellent physicochemical and improved mechanical properties. Additionally, electrodeposition has been widely used in the preparation of this coating based on the characteristics of a simple, cost-effective and green route. The Ni-Co system, owing to its excellent mechanical and chemical performance, has become the major focus of research on composite coatings. It has been reported that the formation of solid-solution strengthening in the alloying of Ni with Co is capable of improved microhardness and enhanced anti-corrosion and wear resistance [1,2]. In recent decades, the incorporation of ceramic nanoparticles (such as Al_2O_3, TiN, ZrO_2 [3–5]) into the metal matrix has caused the expansion of the preparation of composite materials. The incorporation of homogenous particles in growing the metal matrix mainly contributes to decreasing unsought residual stress, improving mechanical properties and extending the longevity of coatings because the composite coating performance mainly relies on the content and distribution of reinforcing particles. However, the incorporation and distribution of a certain number of nanoparticles in composites are difficult because of the agglomeration in the plating bath and settled layer.

The requirement to improve the content and distribution of particles in the plating solution and composites generates the relevancy of research on the effect of assistant methods in deposition. There are various methods for declining the agglomeration and, consequently, for the improvement of the content and degree of particle dispersion in the metal matrix, such as surfactant additives [6], sediment co-deposition [7], pulse electrodeposition [8] or applying different external field, such as mechanical stirring and ultrasonic agitation [9–11].

Among these methods, the application of ultrasound in the electrodeposition process has received much attention and it exhibits extreme potential for use in the industrial field. Various cavitation phenomena (acoustic streaming, microjets, and shock waves [12,13]) caused by ultrasound not only can improve the uniform distribution of particles but also reduce agglomeration in the metal matrix. The choice of the dispersed phase is zirconia, as it is known to possess prominent properties, such as thermal stability, chemical inertness, high hardness and excellent wear and corrosion resistance [14,15]. It has been reported that Ni/ZrO_2 composite coating has been successfully produced by electrodeposition and the trapped zirconia particles effectively improved wear and corrosion resistance [16].

As far as we are aware, nothing about the effects of the different external fields on Ni-Co/ZrO_2 composites' deposition and properties has ever been reported. To this end, we made a comprehensive comparison of Ni-Co/ZrO_2 composite coatings electrodeposited under mechanical stirring (MSED) and ultrasonic agitation (UAED). The coatings were electrodeposited in an aminosulfonate bath with the suspension of ZrO_2 nanoparticles. Additionally, the correlation of the microstructure and the functional properties of the composite coatings were studied in detail.

2. Materials and Methods

2.1. Preparation of Ni-Co/ZrO_2 Composites

Ni-Co/ZrO_2 composite coatings were electrochemically deposited on a mild steel substrate from a standard sulfamate electroplating bath. The bath compositions and plating parameters are shown in Table 1.

Table 1. The bath compositions and plating parameters.

Chemicals	Compositions (g L^{-1})	Plating Conditions
Ni $(NH_2SO_3)_2{\cdot}4H_2O$	80	i = 2.5 A dm^{-2}
Co $(NH_2SO_3)_2{\cdot}4H_2O$	12	pH = 4.0–4.2
H_3BO_3	50	T = 53–55 °C
ZrO_2	10	Time = 2 h

The electrolyte solution was created by adding analytical reagent-level chemicals to distilled water. Figure 1 represents the TEM image of the zirconia nanoparticles, as well as their nanometric sizes (less than 50 nm). The C45 carbon steel substrate with an active area of 6 cm^2 was used as the cathode, and the anode was a nickel sheet with an exposed area of 9 cm^2. Before each experiment, the C45 carbon steel electrode was ground using 600, 800 and 1200 grit sandpapers, and then rinsed with alcohol and distilled water. After that, the sample was activated by a 10 wt% HCl solution for 30 s and rinsed with distilled water.

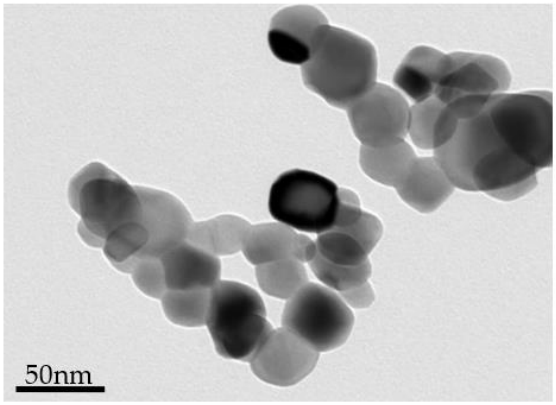


Figure 1. TEM image of ZrO_2 nanoparticles.

Two different external fields were applied in the electrodeposition process of Ni-Co/ZrO_2 composite coatings as follows: mechanical stirring at a speed of 500 rpm, and

the QS12 ultrasonic bath (Ultrawave Ltd.) supplied ultrasonic agitation. There was a built-in thermostat in the ultrasonic bath, which allowed for temperature control up to 70 °C and operated at a frequency of around 35 kHz with an ultrasonic power of 160 to 320 W. To deposit Ni-Co and Ni-Co/ZrO_2 coatings, the mechanical and ultrasonic agitation parameters used are shown in Table 2. The composite coatings' flowcharts for formation are shown in Figure 2 under various external fields.

Table 2. Mechanical and ultrasonic agitation parameters for creating alloy coated samples.

Samples	Compositions	Methods for Treating Electrolyte	
		Mechanical Stirring (rpm)	Ultrasonic Agitation (W)
Sample-I	Ni-Co	500	-
Sample-II	Ni-Co/ZrO_2	500	-
Sample-III	Ni-Co/ZrO_2	-	160
Sample-IV	Ni-Co/ZrO_2	-	240
Sample-V	Ni-Co/ZrO_2	-	320

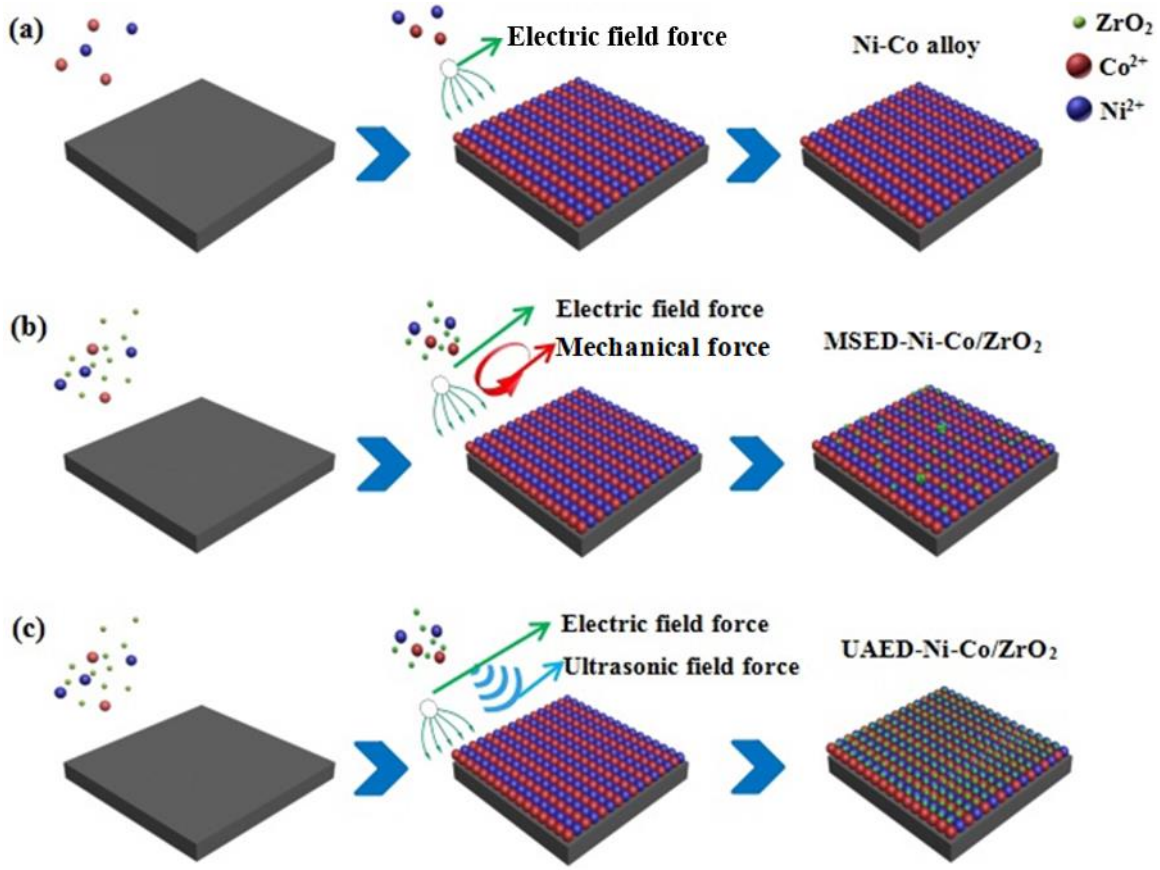


Figure 2. The flowcharts of the composite coatings under different external fields: (**a**) sample-I, (**b**) sample-II, (**c**) sample-IV.

2.2. Characterization of Ni-Co/ZrO_2 Composites

The surface morphology of the coatings was analyzed using a scanning electron microscope (SEM Zeiss- Sigma HD), and the element mass fraction was determined by an energy-dispersive X-ray analyzer (EDX, OXFORD-X-Max). The morphology of zirconia nanoparticles was analyzed by transmission electron microscopy (TEM, JEM-2100). X-ray diffraction was used to investigate the coatings' phase composition and grain structure (X, Pert Powder).

2.3. Electrochemical Analysis

Electrochemical tests of the alloy coated samples were operated in a 0.5 M NaCl experimental solution at a room temperature of 25 °C via electrochemical workstation utilization (AUTOLAB, Metrohm). A conventional single-compartment glass three-electrode cell with a capacity of 25 mL was used to investigate the corrosion resistance of the electrodeposited coatings. A platinum counter electrode was employed as the counter electrode, and a saturated calomel electrode (SCE) was employed as the reference electrode. With an uncovered area of 1.0 cm^2, the prepared coatings were used as working electrodes for corrosion testing. Potentiodynamic polarization curves were scanned at a constant scan rate of 1 mVs^{-1} and measured with mechanical and ultrasonic agitation.

2.4. Friction Measurement

In order to perform the frictional wear test of the alloy coated samples, a corundum ball with a diameter of 1 cm on a ball-on-disc apparatus was used (MS-T3001) at 25 °C under a load of 4 N for 40 min and a rotation of 200 r/min. Subsequently to rotating, the worn surface of the samples was examined using Zeiss-Sigma HD-type field-emission scanning electron microscopy.

2.5. Microhardness Determination

The Vickers hardness of alloy coated samples were measured using a microhardness tester (HX-1000TM/LCD) with an applied load of 200 g for 10 s. Furthermore, the corresponding final values were determined as the average of ten measurements.

3. Results

3.1. Surface Morphology Observation

The surface morphologies of the as-deposited alloy composite coatings obtained under mechanical stirring and ultrasonic agitation are shown in Figure 3. A coarse surface with distinctive spherical granular features can be seen in Figure 3a of the Ni-Co alloy. The surface crystalline size of the Ni-Co/ZrO_2 composite coating produced a mechanical reduction with the incorporation of zirconia as seen in Figure 3b. However, the surface morphology of the Ni-Co/ZrO_2 composite coating still showed a rough surface with some low-sized bulges. The following is shown in Figure 3c–e: the size of grains became refined and the structure of coatings became denser with the application of ultrasonic agitation. It is clear that ultrasound improves the content and distribution of zirconia nanoparticles within the composites; therefore, the coatings became more uniform and compact [17]. Particularly, the Ni-Co/ZrO_2 composite coating produced with ultrasound power of 240 W exhibited the highest level of incorporation and uniformity in the distribution of zirconia particles, smooth surface and dense structure, as shown in Figure 3d. It can be inferred that the ultrasonic agitation reinforces the dispersive strengthening and grain fining effects of nanoparticles, leading to the improvement of surface morphologies [18]. Meanwhile, the cavitation effect of ultrasound can reduce polarization phenomenon of electrolyte, smash the hydrogen bubbles adhered to the cathode, and clean activate surface [19]. However, the increase in roughness of the coatings deposited under the higher ultrasound power (320 W) has been observed. The reason for that could be ascribed to the decrease in the content of nanoparticles embedded in the metal matrix. When the ultrasound power is higher than 240 W, the excessive bath agitation will remove the weakly adsorbed nanoparticles from the cathode surface to the electrolyte [5,20,21]. Therefore, Ni-Co/ZrO_2 composite coating fabricated with an ultrasound power of 240 W was the most favorable for further experiments.

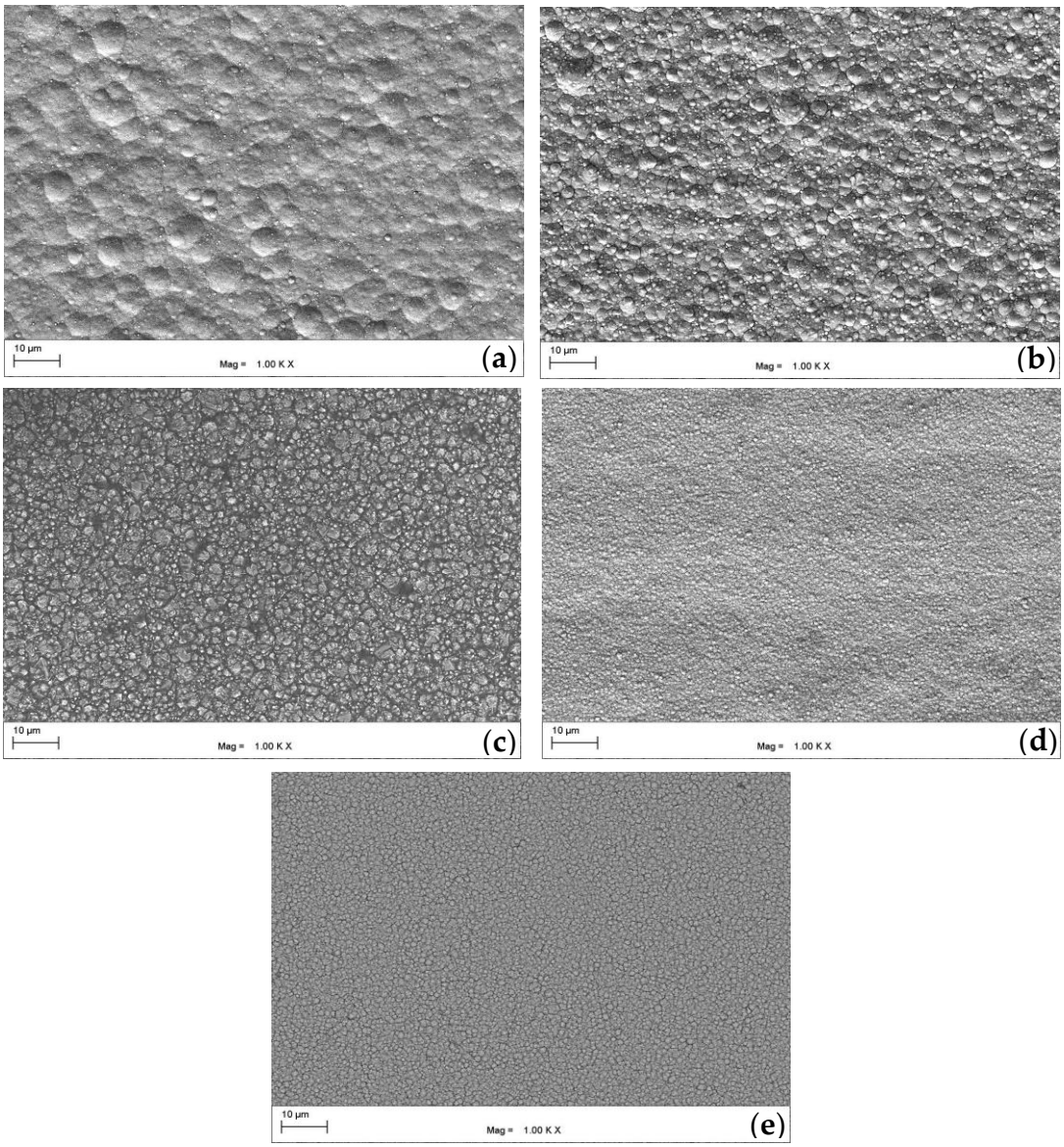


Figure 3. FESEM photographs of coatings prepared under different conditions: (**a**) sample-I; (**b**) sample-II; (**c**) sample-III; (**d**) sample-IV; (**e**) sample-V.

Figure 4 shows the EDS elemental map of the Ni-Co/ZrO_2 composite coatings prepared by different external fields. This detection indicates that the presence of Ni (Figure 4a,d), Co (Figure 4b,e) and Zr (Figure 4c,f) elements was successfully co-deposited into the metal substrate. In the comparison shown in Figure 4c, Zr incorporated into the deposit shown in Figure 4f appears to be more evenly distributed, indicating that the applied stirring of electrolytes has an outstanding influence on the dispersion uniformity of zirconia. It should be noted that the dispersion of nanoparticles has been improved and the agglomeration decreased with the use of ultrasound.

Table 3 shows the elemental analysis of composite coatings fabricated under different external fields. According to Table 3, the zirconia content in the deposits increased significantly upon the increase in ultrasound power from 160 W to 240 W, owing to the cavitation phenomena caused by ultrasound. The increase in zirconia incorporated in the deposit is mainly related to two synergic effects, i.e., the improvement in the particle that migrates to the cathode, and the collision of bubbles that breaks up the agglomeration of the nanoparticles [22,23]. However, as the ultrasound power rose to 320 W, the content of the nanoparticles decreased slightly. This might be due to a decrease in the adsorption

forces between the nanoparticles and the cathode surface under the effect of excessive ultrasonic agitation, affecting the co-deposition quantity of zirconia.

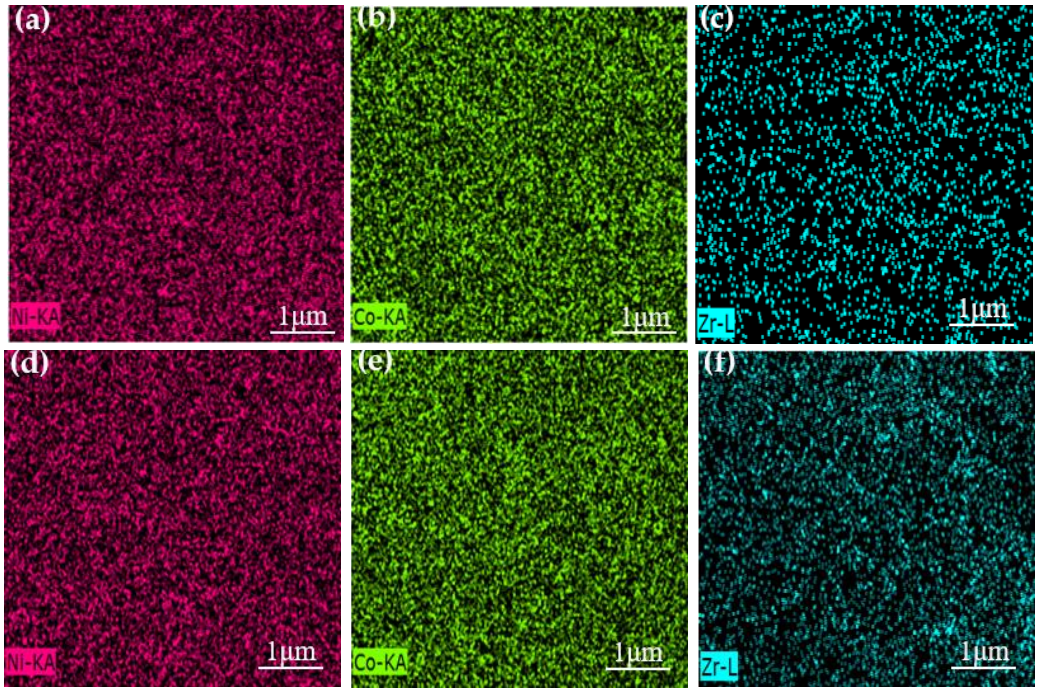


Figure 4. EDS map of Ni-Co/ZrO_2 composite coatings: (**a**–**c**) sample-II; (**d**–**f**) sample-IV.

Table 3. Mass fraction of elements in alloy coated samples prepared under different conditions.

Sample-	Composition in wt%			
	Ni	Co	Zr	O
I	58.4	41.6	-	-
II	56.0	36.4	2.9	4.7
III	59.6	34.0	4.5	1.9
IV	54.8	28.0	7.5	9.7
V	55.7	36.4	4.9	3.0

The FESEM figures of the cross-section of the composite coatings deposited with mechanical stirring (sample-II) and ultrasonic agitation (sample-IV) are shown in Figure 5. The black spot in the left graph represents the agglomeration of zirconia. Figure 5a shows that there exists obvious zirconia aggregation in the MSED-deposited Ni-Co/ZrO_2 composite coating. A lack of visible agglomeration of zirconia is observed in the UAED-deposited Ni-Co/ZrO_2 composite coating with the help of ultrasonic agitation, as shown in Figure 5b. Therefore, the application of ultrasound would effectively depress the agglomeration of nanoparticles and is more suitable to distribute zirconia in the metal substrate during the electrodeposition process. Thickness is one of the important parameters used to evaluate the structure and properties of the coating. The thicknesses of MSED-deposited Ni-Co/ZrO_2 composite coating and UAED-deposited Ni-Co/ZrO_2 composite coating measured by FESEM are 18.73 μm and 14.53 μm, respectively. The combination of process efficiency and coating thickness can better characterize the performance of the coating prepared under certain specific conditions. Therefore, we calculate the process efficiency of the above two coatings, which are 67% and 45%, respectively. Through the comparison of process efficiency, we can obtain results that are consistent with the previous test.

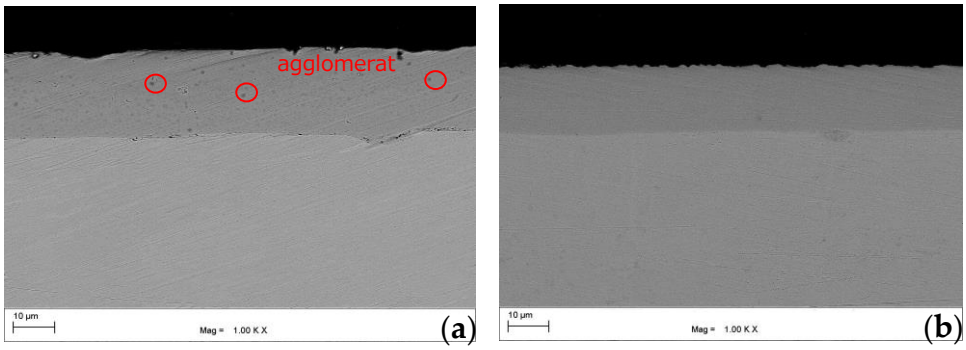


Figure 5. FESEM pictures of the cross-sections of (**a**) sample-II and the (**b**) sample-IV.

Figure 6 depicts the XRD patterns of alloy coated samples prepared under different external fields. Three major characteristic diffraction peaks of NiCo are discriminable at 2θ of 44.4°, 56.8° and 76.3°, and these corresponded to NiCo (111), NiCo (200) and NiCo (220), respectively. The combination of nanoparticles and ultrasound exerted an effect on the diffraction peak intensity and grain structure of the coatings. With the increase in ultrasound power, the diffraction strength of three fiber orientations gradually weakened. This phenomenon is associated with ultrasonic agitation, which enables ZrO_2 to disperse evenly in the plating bath and metal matrix, resulting in the grain strengthening effect and improving the structure of the composite coating [24]. The grain size D was calculated using the Scherrer equation ($D = 0.9\ \lambda/\beta\ \cos\theta$), where λ is the wavelength of the radiation (0.154 nm), β is the full width at half maximum (FWHM) of the peak, and θ is the position of the peak. The grain sizes were found to be 37.5, 33.1, 25.9,19.8 and 24.9 nm for sample-I, II, III, IV and V, respectively.

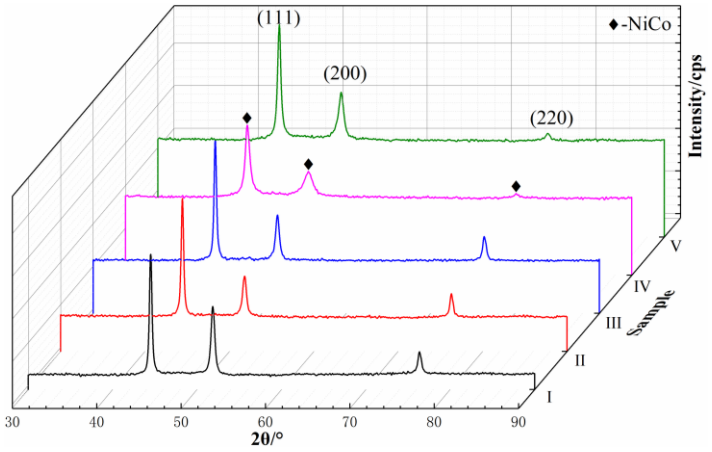


Figure 6. XRD Patterns curves of alloy coated samples prepared under different external fields.

3.2. Microhardness Survey

The microhardness of the alloy coated samples fabricated with mechanical stirring and ultrasonic agitation is presented in Figure 7. All Ni-Co/ZrO_2 composite coatings exhibited higher microhardness than Ni-Co alloys. Specifically, the microhardness of the UAED-deposited Ni-Co/ZrO_2 (160 W) composite coating was 621 HV and, when the ultrasound power reached 240 W, the microhardness of the UAED-deposited Ni-Co/ZrO_2 composite coating increased to 680 HV. Nevertheless, with 320 W of ultrasound power, the UAED-deposited Ni-Co/ZrO_2 composite coating's microhardness decreased to 563 HV. The high value of hardness can be attributed to the following two reasons: on the one hand, the zirconia particles in the deposited coatings obstruct matrix grain boundary migration and the dislocation motion [25]; and on the other hand, the zirconia particles homogeneously incorporated in the metal matrix and the crystal grains were refined,

combined with dispersion strengthening effect [26], leading to high-hardness composite coatings. The intervention of ultrasound in the electrodeposition process improved the dispersion of particles into the alloy matrix; furthermore, it also provoked a refinement in grain size that would lead to an increase in the formation of the nanostructured deposit. As shown in Figure 4f and Table 3, the composite coating obtained the highest microhardness with ultrasound power of 240 W, significantly increasing zirconia uniformly dispersed in the metal matrix. With the incorporation of zirconia with high mass fraction and uniform distribution, which are in good agreement with other researchers [27], we can see from the findings that the microhardness of composite coatings can be significantly enhanced.

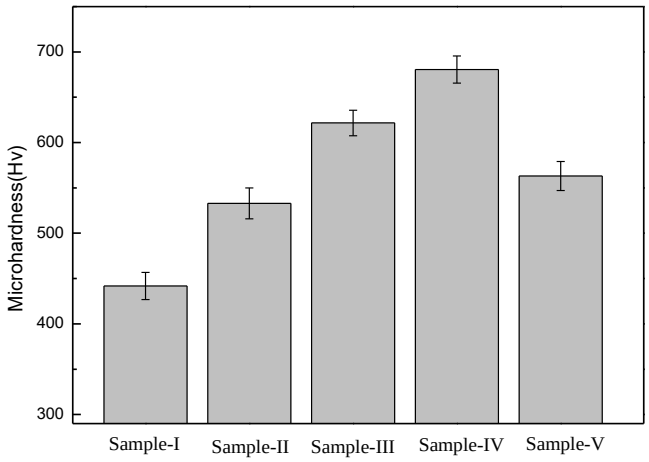


Figure 7. Microhardness curves of alloy coated samples deposited under different external fields.

3.3. Friction Measurement

The alloy coated samples' friction coefficients, as functions of the rotating time, are exhibited in Figure 8. The average friction coefficients were found to be 0.44 ± 0.02, 0.40 ± 0.02, 0.39 ± 0.02, 0.35 ± 0.02 and 0.38 ± 0.02 for sample-I, II, III, IV and V, respectively. It is clear that the UAED-deposited Ni-Co/ZrO_2 composite coatings showed better friction resistance, which indicates that ultrasonic agitation has a significant effect on the tribological mechanism of the coatings. Ultrasonic agitation can better eliminate the agglomeration of nanoparticles in the deposition process so that nanoparticles can be better combined into the coating, forming a more compact composite coating and enabling the coating to more effectively resist external friction. Figure 9 shows the wear loss investigation of the Ni-Co alloy and Ni-Co/ZrO_2 composite coatings. Under ultrasound of 240 W, the sample IV coating was observed to have a minimal mass loss. According to the comparison of Figures 8 and 9, it can be seen that the wear rate increases as its surface hardness decreases, which is in agreement with Archard's equation that the wear rate is inverse-correlated to its surface hardness [28].

It is well known that the wear resistance capability of the coatings depends heavily on the microstructure of the surface and the quantity of ceramic particles added [29]. On the one hand, the UAED-deposited Ni-Co/ZrO_2 composite coatings were denser than the MSED-deposited Ni-Co/ZrO_2 composite coatings and the Ni-Co alloy, which is illustrated in Figure 3. This phenomenon may be conducive to the enhancement of wear resistance. On the other hand, Figures 3–5 illustrate that the zirconia amount in the Ni-Co/ZrO_2 composite coating produced under ultrasound of 240 W was the highest compared to the MSED-deposited Ni-Co/ZrO_2 composite coating and the Ni-Co alloy. Consequently, an increase in content of well-dispersed zirconia particles can effectively enhance the wear resistance of Ni-Co/ZrO_2 composite coating.

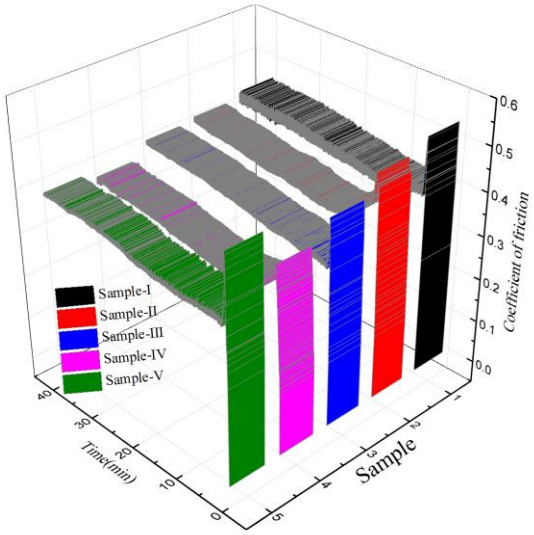


Figure 8. The friction coefficient of Ni-Co alloy and Ni-Co/ZrO_2 composite coatings prepared under different external fields.

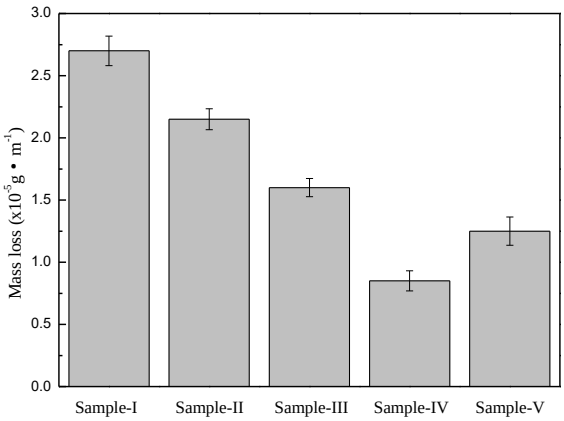


Figure 9. Wear loss curves of alloy coated samples deposited under different external fields.

The surface morphologies of Ni-Co alloy coating and Ni-Co/ZrO_2 composite coating produced under ultrasound of 240 W, and subsequently under wear testing for 40 min, are shown in Figure 10. It can be observed from Figure 10a, for the Ni-Co alloy, that there were obvious wear debris, scratches and grooves on the worn surface, indicating plastic deformation and that a serious adhesive wear mode takes place in the coating. In Figure 10b, the worn surface map of the Ni-Co/ZrO_2 composite coating produced with ultrasound power of 240 W was smooth and clean, showing that this coating had the best wear resistance. Therefore, it can be concluded that the inclusion of zirconia led to a rise in the coatings' wear resistance, which implies that the addition of zirconia nanoparticles plays an important role in the dispersion strengthening effect [30].

3.4. Corrosion Test

Under various conditions, alloy coated samples have potentiodynamic polarization curves, as shown in Figure 11. Table 4 lists the Tafel slopes, corrosion current (i_{corr}) and corrosion potential (E_{corr}) obtained from these curves. The anti-corrosion of the Ni-Co/ZrO_2 composite coating is better than that of the Ni-Co alloy coating, and the corrosion potential of the Ni-Co/ZrO_2 composite coatings produced with ultrasound shifted to more be positive than that of the coating without ultrasonic stirring. With the increase in ultrasound power from 160 to 240 W, E_{corr} shifted positively, whereas i_{corr} decreased noticeably. An explanation for such a shift may be attributed to the modification in grain size and crystal

structure of the composite coatings. The combination of nanoparticles can well prevent the spread of corrosion, that is, the continuation of corrosion and the occurrence of deep corrosion. The nanoparticles acted as physical obstructions to the initiation and spread of corrosion, making the Ni-Co/ZrO_2 composite coatings more corrosion resistant [31,32].

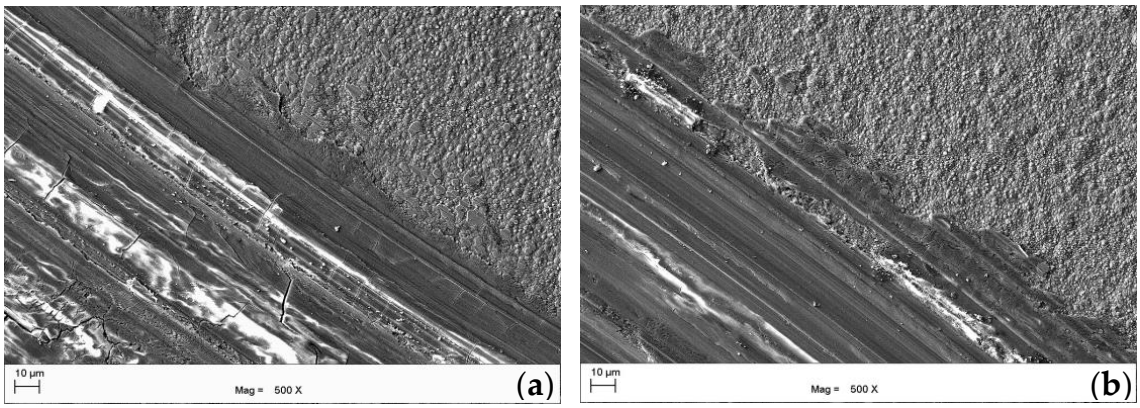


Figure 10. FESEM morphology of the worn surface of two coatings: (**a**) sample-I and (**b**) sample-IV.

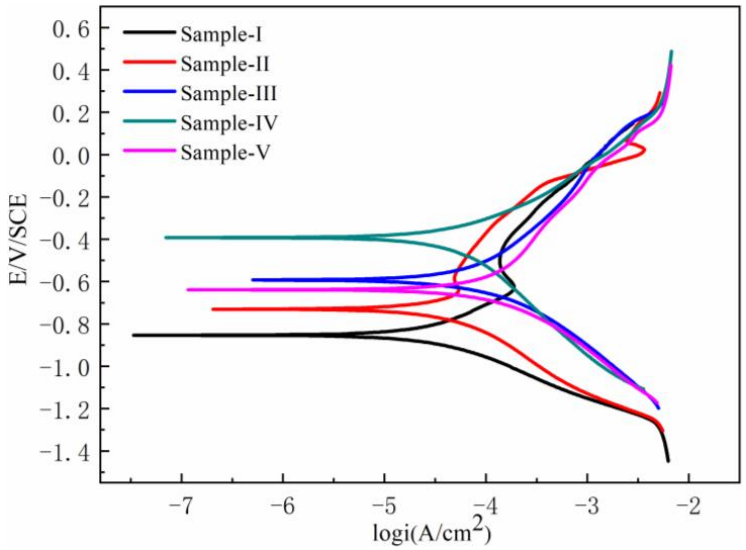


Figure 11. A 0.5 M NaCl solution of alloy coated samples had potential polarization curves.

Table 4. The composite coatings' corrosion potentials and corrosion current densities.

Coating	E_{corr} vs. SCE(V)	i_{corr} (μA/cm^2)	β_a (V/dec)	β_c (V/dec)
I	−0.85	41.34	−0.22	0.35
II	−0.73	30.61	−0.13	0.35
III	−0.59	26.93	−0.13	0.26
IV	−0.39	19.53	−0.10	0.19
V	−0.64	25.57	−0.14	0.20

Additionally, the anodic Tafel slopes (β_a) and cathodic Tafel slopes (β_c) of the Ni-Co/ZrO_2 composite coatings made via ultrasound were lower compared to the alloy coated samples prepared with mechanical stirring. The uniform incorporation of zirconia in the deposits played the main role in improving corrosion behaviors. Due to its compact incorporation and uniform dispersion of zirconia in the matrix, it provides the complicated and longer corrosion routes, thus improving the corrosion resistance of coatings [33]. However, the corrosion resistance property decreased when the ultrasound power was

over 240 W. The occurrence of this phenomenon was ascribed to the decrease in the content of nanoparticles in the composites caused by the receding of the loosely absorbed cathode surface under high ultrasound power. This is in good agreement with previous studies [34,35].

As mentioned above, under ultrasonic agitation, the coatings exhibited smaller grain size, smoother surface, denser structure and higher hardness. Improvement in these parameters usually help to enhance the corrosion protection of composite coatings. Apparently, because of the application of ultrasonic agitation in the deposition, the composites exhibited the distribution of zirconia, and the uniform distribution of zirconia embedded in the composite coatings inactivated the active sites of the corroded surface; therefore, mainly homogeneous corrosion occurs while localized corrosion is inhibited.

4. Conclusions

In this work, the Ni-Co/ZrO_2 composites were electrodeposited from sulfamate electrolytes and the impact of mechanical stirring and ultrasonic agitation on the electrodeposition process and mechanical properties was performed. Additionally, the effect of the different external fields during the deposition process on the morphology, composition distribution, microstructure, microhardness, wear and corrosion resistance of the composite coatings was investigated in detail. The electrodeposition of composites with ultrasonic agitation yielded better surface morphology and mechanical properties than in the case of using mechanical stirring. Mechanical properties, such as microhardness, wear resistance and corrosion resistance, of the composites were decreased due to the increase in ultrasound power. It was demonstrated that ZrO_2 coatings made under ultrasound power of 240 W had the minimum and most compact surface structure.

Author Contributions: B.L. proposed the research topic, investigated and sorted the literature, and obtained research funds; J.S. designed the research program, investigated and collated the literature, conducted the statistical analysis, implemented the research process, designed the framework of the paper; J.L. collected and organized the data, drafted the paper, provided technical and material support, implemented the research process, revised the paper, and provided relevant suggestions; Y.W. designed the research proposal, performed the final review of the paper, and extracted and discussed the conclusions. All authors have read and agreed to the published version of the manuscript.

Funding: This work was supported by the National key Research and Development Program of China (2021YFB3702003).

Institutional Review Board Statement: This article does not contain any studies with human participants performed by any of the authors.

Informed Consent Statement: Not applicable.

Data Availability Statement: All data generated or analysed during this study are included in this published article.

Conflicts of Interest: All authors disclose no relevant relationships.

References

1. Imanian Ghazanlou, S.; Farhood, A.H.S.; Ahmadiyeh, S.; Ziyaei, E.; Rasooli, A.; Hosseinpour, S. Characterization of pulse and direct current methods for electrodeposition of Ni-Co composite coatings reinforced with nano and micro ZnO particles. *Metall. Mater. Trans. A* **2019**, *50*, 1922–1935. [CrossRef]
2. Dietrich, D.; Scharf, I.; Nickel, D.; Shi, L.; Grund, T.; Lampke, T. Ultrasound technique as a tool for high-rate incorporation of Al2O3 in NiCo layers. *J. Solid State Electrochem.* **2011**, *15*, 1041–1048. [CrossRef]
3. Zahra, S.; Bahrololoom, M.E.; Hashemi, B. Electrodeposition of nanocrystalline Ni/Ni-Al_2O_3 nanocomposite modulated multilayer coatings. *Mater. Des.* **2016**, *108*, 19–26.
4. Guo, Y.X.; Liu, Q.B.; Shang, X.J. In situ TiN-reinforced CoCr2FeNiTi0.5 high-entropy alloy composite coating fabricated by laser cladding. *Rare Metals* **2020**, *39*, 1190–11955. [CrossRef]
5. Beltowska-Lehman, E.; Indyka, P.; Bigos, A.; Szczerba, M.J.; Kot, M. Ni–W/ZrO_2 nanocomposites obtained by ultrasonic DC electrodeposition. *Mater. Des.* **2015**, *80*, 1–11. [CrossRef]

6. Chiu, S.Y.; Chung, S.T.; Lin, C.Y.; Tsai, W.T. Electrodeposition of Ni-Al_2O_3 composite coatings employing supercritical CO_2 baths. *Surf. Coat. Technol.* **2014**, *247*, 68–73. [CrossRef]
7. Rahman, M.T.; Hoque, M.A.; Rahman, G.T. Evaluation of thermal, mechanical, electrical and optical properties of metal-oxide dispersed HDPE nanocomposites. *Mater. Res. Express.* **2019**, *6*, 085092. [CrossRef]
8. Karimzadeh, A.; Aliofkhazraei, M.; Rouhaghdam, A.S. Study on wear and corrosion properties of functionally graded nickel-cobalt-(Al_2O_3) coatings produced by pulse electrodeposition. *Bull. Mater. Sci.* **2019**, *42*, 53. [CrossRef]
9. Mousavi, R.; Bahrololoom, M.E.; Deflorian, F.; Ecco, L. Improvement of corrosion resistance of Nisingle bondMo alloy coatings: Effect of heat treatment. *Mater. Des.* **2016**, *364*, 9–14.
10. Nan, T.X.; Yang, Y.G.; Chen, B. Electrochemical mechanism of tin membrane electrodeposition under ultrasonic waves. *Ultrason. Sonochem.* **2018**, *42*, 731–737. [CrossRef]
11. Ünal, E.; Karahan, İ.H. Effects of ultrasonic agitation prior to deposition and additives in the bath on electrodeposited Ni-B/hBN composite coatings. *J. Alloys Compd.* **2018**, *763*, 329–341. [CrossRef]
12. Rahman, M.T.; Hoque, M.A.; Rahman, G.T. Study on the mechanical, electrical and optical properties of metal-oxide nanoparticles dispersed unsaturated polyester resin nanocomposites. *Results Phys.* **2019**, *13*, 102264. [CrossRef]
13. Tudela, I.; Zhang, Y.; Pal, M.; Kerr, I.; Cobley, A.J. Ultrasound-assisted electrodeposition of composite coatings with particles. *Surf. Coat. Technol.* **2014**, *259*, 363–373. [CrossRef]
14. Bapu, G.N.K.R.; Jayakrishnan, S. Oxidation characteristics of electrodeposited nickel–zirconia composites at high temperature. *Mater. Chem. Phys.* **2006**, *96*, 321–325. [CrossRef]
15. Zhang, K.F.; Ding, S.; Wang, G.F. Different superplastic deformation behavior of nanocrystalline Ni and ZrO2/Ni nanocomposite. *Mater. Lett.* **2008**, *62*, 719–722. [CrossRef]
16. Arghavanian, R.; Ahmadi, N.P.; Yazdani, S.; Bostani, B. Investigation on corrosion proceeding path and EIS of Ni-ZrO2 composite coating. *Surf. Eng.* **2012**, *28*, 508–512. [CrossRef]
17. Gyawali, G.; Cho, S.H.; Woo, D.J.; Lee, S.W. Pulse electrodeposition and characterisation of Ni–SiC composite coatings in presence of ultrasound. *Trans. IMF* **2013**, *90*, 274–281. [CrossRef]
18. Chang, L.M.; Guo, H.F.; An, M.Z. Electrodeposition of Ni-Co/Al_2O_3 composite coating by pulse reverse method under ultrasonic condition. *Mater. Lett.* **2008**, *62*, 3313–3315. [CrossRef]
19. Hovestad, A.; Janssen, L.J. Electrochemical codeposition of inert particles in a metallic matrix. *J. Appl. Electrochem.* **1995**, *25*, 519–527. [CrossRef]
20. Wang, Y.; Liang, Z.; Zhou, X.; Jin, H. Electrochemical and Tribological Behavior of Ni-Co/ZrO_2 Coatings Prepared by Ultrasound-Assisted Electrodeposition. *Int. J. Electrochem. Sci.* **2018**, *13*, 9183–9199. [CrossRef]
21. Su, F.; Liu, C.; Huang, P. Ultrasound-assisted pulse electrodeposition and characterization of Co–W/MWCNTs nanocomposite coatings. *Appl. Surf. Sci.* **2014**, *309*, 200–208. [CrossRef]
22. García-Lecina, E.; García-Urrutia, I.; Díez, J.A.; Morgiel, J.; Indyka, P. A comparative study of the effect of mechanical and ultrasound agitation on the properties of electrodeposited Ni/Al_2O_3 nanocomposite coatings. *Surf. Coat. Technol.* **2012**, *206*, 2998–3005. [CrossRef]
23. Zheng, H.Y.; An, M.Z. Electrodeposition of Zn–Ni–Al_2O_3 nanocomposite coatings under ultrasound conditions. *J. Alloys Compd.* **2008**, *459*, 548–552. [CrossRef]
24. Wang, M.; Li, W.L.; Feng, Y.; Hou, Y.F.; Xu, D.; Wang, M.; Fei, W.D. In-situ X-ray diffraction study of stress-induced phase transition of (1 − x) $BaZr_{0.2}Ti_{0.8}O_3$–x$Ba_{0.7}Ca_{0.3}TiO_3$ in polymer matrix composite. *Mater. Chem. Phys.* **2014**, *146*, 431–436. [CrossRef]
25. Wang, Y.; Wang, H.; Li, C.S.; Feng, J.Q.; Jin, L.H.; Yu, Z.M.; Odier, P.; Zhang, P.X. Effective removal procedure of residual carbon in CeO_2−x films fabricated via MOD method. *Ceram. Int.* **2015**, *41*, 14270–14275. [CrossRef]
26. Singh, D.K.; Tripathi, M.K.; Singh, V.B. Electrolytic Preparation of Ni-B_4C Composite Coating and its Characterization. *J. Mater. Eng. Perform.* **2015**, *24*, 1213–1219. [CrossRef]
27. Su, F.; Liu, C.; Guo, J.; Huang, P. Characterizations of nanocrystalline Co and Co/MWCNT coatings produced by different electrodeposition techniques. *Surf. Coat. Technol.* **2013**, *217*, 94–104. [CrossRef]
28. Sun, W.C.; Gu, J.W.; Zhang, P.; Tian, M.M.; Wang, Y.; Cai, H.; Hu, S.F. Fabrication and High Temperature Friction Behavior and Oxidation Resistance of Ni-Co-ZrO_2 Composite Coating. *Mater. Res.* **2016**, *19*, 562–571. [CrossRef]
29. Allahkaram, S.R.; Golroh, S.; Mohammadalipour, M. Properties of Al_2O_3 nano-particle reinforced copper matrix composite coatings prepared by pulse and direct current electroplating. *Mater. Des.* **2011**, *32*, 4478–4484. [CrossRef]
30. Protsenko, V.S.; Danilov, F.I. Kinetic model of composite coatings electrodeposition assuming irreversible adsorption of dispersed particles on a growing metal substrate. *J. Electroanal. Chem.* **2022**, *918*, 116463. [CrossRef]
31. Yang, X.K.; Li, Q.; Zhang, S.Y.; Zhong, X.K.; Dai, Y.; Luo, F. Electrochemical corrosion behaviors and protective properties of Ni–Co–TiO2 composite coating prepared on sintered NdFeB magnet. *Mater. Corros.* **2010**, *61*, 618–625. [CrossRef]
32. Baghery, P.; Farzam, M.; Mousavi, A.B.; Hosseini, M. Ni–TiO_2 nanocomposite coating with high resistance to corrosion and wear. *Surf. Coat. Technol.* **2010**, *204*, 3804–3810. [CrossRef]
33. Bakhit, B.; Akbari, A. Effect of particle size and co-deposition technique on hardness and corrosion properties of Ni–Co/SiC composite coatings. *Surf. Coat. Technol.* **2012**, *206*, 4964–4975. [CrossRef]

34. Tudela, I.; Zhang, Y.; Pal, M.; Kerr, I.; Cobley, A.J. Ultrasound-assisted electrodeposition of thin nickel-based composite coatings with lubricant particles. *Surf. Coat. Technol.* **2015**, *276*, 89–105. [CrossRef]
35. Camargo, M.K.; Tudela, I.; Schmidt, U.; Cobley, A.J.; Bund, A. Ultrasound assisted electrodeposition of Zn and Zn-TiO2 coatings. *Electrochim. Acta* **2016**, *198*, 287–295. [CrossRef]

Disclaimer/Publisher's Note: The statements, opinions and data contained in all publications are solely those of the individual author(s) and contributor(s) and not of MDPI and/or the editor(s). MDPI and/or the editor(s) disclaim responsibility for any injury to people or property resulting from any ideas, methods, instructions or products referred to in the content.